ISSN 1027-4510, Journal of Surface Investigation: X-ray, Synchrotron and Neutron Techniques, 2020, Vol. 14, No. 4, pp. 851–861. © Pleiades Publishing, Ltd., 2020.

α-$FeSi_2$ as a Buffer Layer for β-$FeSi_2$ Growth: Analysis of Orientation Relationships in Silicide/Silicon, Silicide/Silicide Heterointerfaces

I. A. Tarasov[a], I. A. Bondarev[a, *], and A. I. Romanenko[b]

[a] *Kirensky Institute of Physics, Federal Research Center KSC SB RAS, Krasnoyarsk, 660036 Russia*

[b] *Nikolaev Institute of Inorganic Chemistry, SB RAS, Novosibirsk, 630090 Russia*

**e-mail: bia@iph.krasn.ru*

Received December 24, 2019; revised January 17, 2020; accepted January 19, 2020

Abstract—In this manuscript, we attempt to clarify the capability of utilisation of α-$FeSi_2$ nanocrystals as a buffer layer for growth of monocrystalline/high-quality β-$FeSi_2$ direct-gap semiconductor from the point of view of the crystal lattice misfits and near coincidence site (NCS) lattices. Iron silicides-based nanostructures have a wide spectrum of possible industrial applications in different fields. Mainly, interest in these functional materials is caused by their ecological safety and Earth's core abundance that give us the opportunity for greener future with highly effective electronic devices. β-$FeSi_2$ phase due to its allowed direct transition with energy close to 0.87 eV can be used as active material in light emission diodes (LED). Utilisation of buffer layers between silicon substrate and give one more tool to engineer the band structure of semiconducting β-$FeSi_2$ phase. We attempt to clarify the capability of the utilisation of the α-$FeSi_2$ phase as a buffer layer for the growth of β-$FeSi_2$ direct-gap semiconductor from the point of view of the crystal lattice misfits and near coincidence site (NCS) lattices. Possible β-$FeSi_2$/α-,γ-,s-$FeSi_2$/Si orientation relationships (ORs) and habit planes were examined with crystallogeometrical approaches and compared with β-$FeSi_2$/Si ones. The lowest interplanar and interatomic spacing misfits between silicon lattice and a silicide one are observed for the pair of s-$FeSi_2${011}[200]/Si{022}[100] at room temperature and equal to –0.57%. The least interplanar and interatomic spacing misfit of 1.7 and 1.88%, respectively, for β-$FeSi_2$/Si, can be decreased as low as –0.67 (interplanar) and 0.87 (interatomic) % by placing an α-$FeSi_2$ layer between silicon and β-$FeSi_2$ phase. It is stated that the growth of metastable γ-$FeSi_2$ is also favourable on silicon due to low interplanar and interatomic spacing misfit (–0.77%) and a higher density of NCS in comparison with s-$FeSi_2$. Design and technological procedure for the synthesis of possible β-$FeSi_2$/α-$FeSi_2$/Si heterostructure have been proposed based on the results obtained.

Keywords: iron silicide, interface structure, orientation relationship, near coincidence site lattice, edge-to-edge matching, plane-to-plane matching

DOI: 10.1134/S1027451020040357

1. INTRODUCTION

Iron silicides-based nanostructures have a wide spectrum of possible industrial application in different fields. Mainly, interest in these functional materials is caused by their ecological safety and Earth's core abundance that give us the opportunity for greener future with highly effective electronic devices. Ferromagnetic silicides, i.e. Fe_3Si [1], Fe_5Si_3 [2] and other non-stoichiometric iron-silicon alloys $Fe_{1-x}Si_x$ [3], are prominent for production of spintronic devices due to their high level of spin polarisation. Semiconducting β-$FeSi_2$ phase can be utilised as the active material in photon crystals [4], for photovoltaics [5, 6], thermoelectrics [7, 8] and also for electric charge storage [9]. Finally, β-$FeSi_2$ phase due to its allowed direct transition with energy close to 0.87 eV can be used as active material in light emission diodes (LED) [10]. In spite overcoming the issue of enhancing the luminescence of β-$FeSi_2$—based LED, which has been at the aim of many research groups [11–17], such diodes are still unavailable in the market for wide consumption. The highest values for output optical power and external quantum efficiency reported before lie in the range from 25 μW [16] to 420 μW [17], and from 0.009% [16] to 0.12% [17], respectively. Thus, the intensity of room temperature β-$FeSi_2$ IR luminescence is currently inferior to that of InGaAs compounds [12, 18].

On the other side, self-assembling β-$FeSi_2$ single-crystalline nanowires/nanowhiskers/nanocrystals with engineered band structure could improve it to reach 1.5 μm light emission as high as the commercial analogues have. Reducing dimensions of β-$FeSi_2$ down to nanoparticles embedded in silicon matrix

with diameters about 20 nm has already shown a great potential for the enhancement of IR photoluminescence and electroluminescence in comparison with β-$FeSi_2$ thin films [12, 16]. The nanoscale size of the β-$FeSi_2$ crystals allows them to be stressed using a silicon matrix in such a way as to provide a defect-free interface, and which promotes a low concentration of non-radiative recombination centres. Thereby it allows one to change β-$FeSi_2$ band structure due to different orientation relationship (OR). As a continuation of this idea, the growth of epitaxial freestanding β-$FeSi_2$ nanowires on silicon substrate could allow one to possess a bigger volume of relaxed defect-free β-$FeSi_2$ phase. Such benefits, as low leakage current [19], tuning emission directionality [20], which are given by high aspect ratio and homogeneous spatial alignment of nanowires/nanowhisker, are expected. Nevertheless, there are few reports concerning the growth of such epitaxial freestanding β-$FeSi_2$ nanocrystals [21–24] and even less showing the formation of such structures on a silicon substrate. One of the reason is high lattice mismatches between β-$FeSi_2$ and silicon [22, 25].

To achieve the formation of such Si-β heterostructures one may consider utilising intermediates [26]. This intermediate can be found among other disilicides phases, such as tetragonal α-$FeSi_2$, cubic CaF_2-type γ-$FeSi_2$ and CsCl-type *s*-$FeSi_2$ (or $Fe_{0.5}Si$), having better OR with silicon [22]. However, despite the idea was suggested by Y. Gao et al. [26] in 2008, any substantial attempt aimed to shed light on this problem, which of α -, γ- or *s*-disilicide phases is more favourable for further self-assembling β-$FeSi_2$ growth, has not been done yet. Self-assembled $FeSi_2$ silicide buffer nanocrystal ensembles could serve as formation centres for β-$FeSi_2$ nanowhiskers in analogy with the vapour-liquid-crystal mechanism, like in case of Si nanowires growth on the gold-activated surface. The effect of nanowires growth activation by the catalyst particles is that the growth processes on the surface under a catalyst droplet proceeds much faster than on a non-activated surface. Here, the transition of the material from vapour to liquid takes place, and as a result, the solution becomes supersaturated and crystallises on the surface under the droplet. Whereas faster growth of the β-$FeSi_2$ phase on the buffer α-, γ- or *s*-$FeSi_2$ precipitates/nanocrystals can be presumably achieved by lowering their joint interface energy in comparison with buffer-nanocrystal-free-silicon surface. To suppress the formation of β-$FeSi_2$ phase on silicon the selective oxidation can be applied. Therefore, it is important to know which surfaces of α- (or) γ- (or) *s*-$FeSi_2$, orientation relationships and synthesis conditions are the most favourable for subsequent freestanding epitaxial β-$FeSi_2$ nanowires growth.

To date, the formation of cubic γ- *s*-$FeSi_2$ silicides by different physical and chemical methods was widely reported [22, 27–31]. Thus, two monolayers (ML) of pure Fe followed by codeposition of Fe and Si at a stoichiometric ratio (1 : 1) onto Si(111) surface at a temperature less than 100°C resulted in CsCl-like $Fe_{1-x}Si$ (*s*-$FeSi_2$) formation [27]. The *s*-$FeSi_2$ endotaxial NWs growth was also reported due to reactive deposition at 700°C of Fe 2 ML onto Si(110) [22]. Das et al. showed that different coverages of Fe up to 2 ML deposited on Si(110) substrate at the temperature of 600°C results in forming endotaxial γ-$FeSi_2$ NWs [31]. In turn, annealing at 500°C of Fe from 2 to 5 ML deposited on Si(111) forms γ-$FeSi_2$ [30]. Goldfrab et al. [28] has recently shown the annealing of Fe coverage of no more than 10 MLs on Si(001) and Si(111) substrates in the temperature range from 500 to 750°C results in the formation of the γ-$FeSi_2$ nanoislands with different size and shapes and orientations, which strongly affect their magnetic response. It is general for these metastable phases to transform to β-$FeSi_2$ or ε-FeSi phases when nominal thickness reaches the values 1.5–2 nm [22].

In turn, forming of the epitaxial α-$FeSi_2$ thin film via pulsed laser deposition [32], annealing of prior deposited Fe film [33, 34], ion implantation [35], polycrystalline film via facing target radio-frequency magnetron sputtering method [36], and subsequent Fe deposited layer annealing [37] were reported. Self-assembled α-$FeSi_2$ nanocrystals were synthesised on Si(100), and Si(111) surfaces by ion implantation [26], solid-phase epitaxy [38], and microwave plasma-assisted chemical vapour deposition [39]. It was reported the endotaxial α-$FeSi_2$ NWs are grown by deposition Fe on Si(110) at 650°C [40], whereas under similar conditions (600 and 700°C) the growth of s-$FeSi_2$ and γ-$FeSi_2$ phases were reported, respectively [22, 31]. Despite the fact that α-$FeSi_2$ is considered to be a metastable phase in bulk, below 915–960°C it transforms into the β-$FeSi_2$ phase according to the eutectoid reaction α-$FeSi_2 \rightarrow \beta$-$FeSi_2$ + Si [41], several reports about crystal structure and physical properties of the single bulk crystal and polycrystalline samples exist.

Here we attempt to estimate and predict ORs and habit planes between α-, γ-, *s*-$FeSi_2$ and β-$FeSi_2$ phases with the help of crystallogeometrical approaches. These approaches suppose that the habit plane formation and orientation relationship between two crystal structures are regulated by a decrease in the interface energy, where lower interface energy corresponds to habit planes with a high degree of atomic site matching. However, application of these methods is not suitable for the systems with the high anisotropy of the surface energy. These methods for the analysis of the interphases boundaries for nanoscale objects not

involving *ab initio* calculations can be sophisticated as follows (1) a purely geometrical, (2) a rigid model energetic, and (3) an extension of (2), in which elastic relaxation is included [42]. Furthermore, atomistic simulations with empirical interatomic potentials have been demonstrated to be reliable to explore energy minimisation mechanism of semi-coherent interfaces [43].

Thus, crystallogeometric models as plane-to-plane, edge-to-edge approaches, which are elaborately explained in [44, 45], and consideration of the near coincidence site lattice concept [46] are implemented to find the most suitable ones for the self-assembling β-$FeSi_2$ nanocrystal growth. Basic and interface orientation relationships are under consideration.

2. RESULT AND DISCUSSION

2.1. Consideration of the Best Matching Interplanar and Interatomic Spacings in Si//α-, β, γ-, s-$FeSi_2$ and β-$FeSi_2$//α-, γ-, s-$FeSi_2$ Heterosystems

Better orientation relationships of α-, γ-, *s*-$FeSi_2$ compounds with silicon in comparison with the β-$FeSi_2$ result from their higher symmetry group. The γ-$FeSi_2$ phase has cubic fcc (*Fm3m*) CaF_2 structure with lattice constant a = 5.389 Å [22]. The *s*-$FeSi_2$ phase, which is rarely reported in the literature available, possesses cubic bcc (*Pm3m*) structure of the defect CsCl with a lattice constant of 2.7 Å [22]. The α-$FeSi_2$ phase belong to lower tetragonal crystal system (*P*4*mmm*) with lattice parameters a, b = 2.684 Å, c = 5.128 Å [47]. The β-$FeSi_2$ phase has the lowest crystal system among the $FeSi_2$ phase family. It is characterised with a base-centered orthorhombic structure with *Cmca* space group (a = 9.88 Å, b = 7.79 Å, and c = 7.83 Å) [48]. In order to find out which $FeSi_2$ compound would act better as a buffer layer between the silicon substrate and β-$FeSi_2$ phase to diminish its lattice strain, we attempt to carry out the misfit analysis of the different combination of β-$FeSi_2$/buffer layer/Si heterostructures with the help of crystallogeometrical approaches. Two crystallographic models, namely, edge-to-edge and direct lattice matching were used to carry out misfit analysis and predict possible atomic arrangements in such heterostructures. For calculations, we used free and open-source software “phase transformation crystallography PTC Lab” [49]. The edge-to-edge matching model consists of two steps; the first is to find possible close-packed direction (atomic rows) in two crystals. The second step is to find good matching planes containing the atomic rows determined during the first step. The most important feature of this arrangement is that the edges of the planes must consist of the required close-packed or nearly close-packed atom rows in each phase [44]. These planes with similar d spacing may not be parallel to each other and merely bring the atoms rows together at the interface. Direct lattice matching method is based on the same rule, which is to find two pairs of good matching directions between two crystals with a high packing density.

Thus, here we only focus on the geometrical approach of the α-, β-, γ-, *s*-$FeSi_2$ and Si favourable orientation relationship analysis. The question of prediction of interface formation between two phases is rather difficult, in case of the β-$FeSi_2$/Si interface the quantity of possible OR and habits planes exceeds a dozen [25]. This estimation based on an only geometrical criterion, despite its simplicity, has already proved its efficiency [44–46, 50–54], and here it is intended to obtain useful information for our further technological work on synthesis, tailoring the structure and morphology design of the $FeSi_2$ nanostructures [55–58]. Nevertheless, such detailed research on the problem of interface formation in β-$FeSi_2$/α-, γ-, *s*-$FeSi_2$/Si heterostructures including a combination of crystallogeometrical and DFT approaches is planned in the short term.

Table 1 contains interatomic and interplanar spacing misfit values for different combinations of atomic planes and rows in pairs of Si/α-, β-, γ-, s-$FeSi_2$ and β-$FeSi_2$ and α-, γ-, *s*-$FeSi_2$ compounds. Such basic ORs are aimed to show and compare the lowest possible misfit between silicon/silicide different plane and direction pair. They represent a case when planes and directions are parallel but do not reveal information about habit planes. Even though the edge-to-edge and direct lattice matching methods can predict the interface ORs, we do not consider in detail here possible habit planes for all combinations of silicide/silicide/silicon. However, the most favourable ones for good epitaxial alignment combination, based on analysis of the misfit values (Table 1), will be examined closer below. Misfit value δ for phase b growing on phase a is determined with expression $\delta = (d_b - d_a)/d_a \times$ 100%. The combination of directions and planes with misfit higher 4% was excluded from the table. As one could expect the cubic silicides *s*-$FeSi_2$ (defect CsCl-like structure) and γ-$FeSi_2$ (CaF_2) have the smallest interatomic misfit values with silicon at room temperature, –0.57 and –0.77%, between $\langle 100\rangle_{Si}$ and $\langle 200\rangle_s$, $\langle 100\rangle_{Si}$ and $\langle 100\rangle_\gamma$, respectively. For these phases epitaxial interphase boundary, habit planes are expected to be low-index crystal planes, where good coincidence of the planes Si{022}//s-$FeSi_2${011}, γ- $FeSi_2${022} and Si{002}//s-$FeSi_2${001}, γ-$FeSi_2${002} of –0.57 and –0.77%, will determine an epitaxial alignment of the interface with 2D periodicity [37]. The α-$FeSi_2$ compound demonstrates larger misfit values –1.17% with silicon for Si{022}//α{110} planes and same indexed directions. Due to lower symmetry, this phase reveals another possible combination as well, Si{022}//α{012}, with

Table 1. Calculated interatomic and interplanar spacing misfit between α-, β-, γ-, s-$FeSi_2$ and silicon crystal structures at room temperature

Interplanar spacing misfit, %	Matching planes					Interatomic spacing misfit, %	Close-packed rows of atoms				
	Si	β	α	γ	*s*		Si	β	α	γ	*s*
Silicon//α-,β,γ-,*s*-$FeSi_2$											
−0.57	{022}				{011}	−0.57	⟨100⟩				⟨200⟩
−0.77	{022}			{022}		−0.77	⟨100⟩			⟨100⟩	
−1.17	{022}		{110}			−1.17	⟨011⟩		⟨220⟩		
−1.17	{022}		{110}			−2.73	⟨111⟩		⟨221⟩		
−3.56	{022}		{012}			−1.12	⟨100⟩		⟨200⟩		
1.7	{022}	{040}				1.7	⟨011⟩	⟨010⟩			
1.88	{022}	{004}				1.8	⟨011⟩	⟨001⟩			
−4.25	{022}	{422}				−1.82	⟨200⟩	⟨011⟩			
β-$FeSi_2$//α-,γ-,*s*-$FeSi_2$											
−0.4		{008}	{123}			−1.32		⟨110⟩	⟨222⟩		
−0.67		{422}	{012}			2.83		⟨010⟩	⟨220⟩		
−0.67		{422}	{012}			1.03		⟨102⟩	⟨442⟩		
−0.67		{422}	{012}			0.87		⟨120⟩	⟨442⟩		
2.25		{040}			{011}	2.43		⟨001⟩			⟨022⟩
2.43		{004}			{011}	2.25		⟨010⟩			⟨022⟩
2.45		{040}		{022}							
2.63		{004}		{022}							
2.83		{040}	{110}			3.03		⟨001⟩	⟨022⟩		
3.03		{004}	{110}			2.83		⟨010⟩	⟨022⟩		
−3.04		{422}	{110}			−0.89		⟨120⟩	⟨442⟩		
−3.45		{422}		{022}							
−3.66		{422}			{011}						

misfit value −3.56%, which could also regulate interface structure alignment. In turn, β-$FeSi_2$ phase has a positive misfit value of 1.77 and 1.88% for β{040}//Si{022} and for β{004}//Si{022}, respectively. This value is 1.5 larger than for the α-$FeSi_2$ phase. In case of the epitaxy β-$FeSi_2$ crystal structure turns to be under compression that is less favourable for the growth than positive tensile strain conditions corresponded to α-, γ, *s*-$FeSi_2$ formation on silicon. Lattice correspondence of β-$FeSi_2$ with other $FeSi_2$ silicide compounds demonstrates worse misfit values for β{040} planes. The misfit values are positive and varies from 2.25% for *s*-$FeSi_2$ and up to 3.03% in case of α-$FeSi_2$ phase, in case of Si{022}//β{040} δ = 1.77%. It is clear that such a situation appears due to α-, γ-, *s*-$FeSi_2$ are shrunk, and β-$FeSi_2$ is extended concerning silicon. Nevertheless, the tetragonal symmetry of α-$FeSi_2$ results in that α{012} plane having the highest density of atoms packed and demonstrates the lowest misfit value (−0.67%) with β(422), where β{422} plane has the highest density of atoms in the β-$FeSi_2$ compound as well. Whereas the {022} planes in cubic silicon and γ-, *s*-$FeSi_2$ silicides equivalent to {012} plane in tetragonal structure of α-$FeSi_2$ (*P*4*mmm*) have misfit values lower than −3%. Moreover, considering planes with lower atomic density α{123} with structure factor of ~13% even lower misfit value (−0.4%) is obtained. Thus, β-$FeSi_2$/α-$FeSi_2$/Si heterostructure seems to be favourable to achieve a good epitaxial condition for a less strained β-$FeSi_2$ phase.

2.2. NCS Maps of Habit Planes for β-$FeSi_2$/α-$FeSi_2$ and β-$FeSi_2$/Si Heterosystems

Experimental examinations of β-$FeSi_2$ thin film growth on silicon reveal that the following basic ORs of habit planes β(101)‖Si(111), β(110)‖Si(111) are typical for β-$FeSi_2$ epitaxy on (111) silicon surface. The misfits along $[112]_{Si}$, $[011]_{Si}$ directions with β-$FeSi_2$

are −5.6% and + 1.7%. For the $\beta(110)\|Si(111)$ case the misfits are −5.6% and +1.88% (Table 1). These ORs are characterised with the rectangular symmetry of $\beta(110)$, $\beta(101)$ planes, that due to their superimposition with hexagonally symmetric Si(111) plane can potentially bring about the formation of three equivalent domains during the β-$FeSi_2$ film growth (Fig. 1). In case of Si(100) epitaxy two types of ORs are frequently reported, Type A β-$FeSi_2(100)[010] \parallel Si(100)\langle 011\rangle$ and type B: β-$FeSi_2$ $(100)[010]\|Si(100)\langle 001\rangle$. The misfits along these directions are 1.7 and −4.3%, respectively. It worth noting that the most favourable basic ORs obtained above (Table 1) for β-$FeSi_2$ and silicon correspond to the experimental ones.

When two atomic planes with the same symmetry and lattice parameter are superimposed with some rotation and translation, a kind of superstructure, a coincidence site lattice develops. However, in general case, a coincidence site lattice may not exist, and only a near coincidence site lattice can be built, where the criterion of coincidence is an adjustable parameter. Thus, it would be informative to compare the density of near coincidence sites (NCS) in these conventional habit planes in two cases $\beta\|\alpha$ and $\beta\|Si$ (Fig. 1). The $\alpha\{112\}$ plane equivalent to Si{111} instead of $\alpha\{111\}$ were taken for further consideration from the point of view of interplanar distance and atom density. The criterion for the near coincidence site was chosen as 10.8% (~0.59 Å) of silicon lattice parameter at room temperature (RT). Such a small value was used to be able to distinguish the difference between Si and α-$FeSi_2$ in NCS density on a relatively small area (20 × 60 Å). The NCS density is the ratio between a quantity of NCS in habit plane and the number of atoms in silicon or α-$FeSi_2$ compound.

The $\beta\{110\}\|Si\{111\}$ and $\beta\{101\}\|Si\{111\}$ ORs show slight difference in NCS density, 0.098 and 0.083, respectively, whereas in case of $\beta\|\alpha$ superimposition NCS density increases up almost twice, 0.1875. This is caused by the lower density of atoms in $\alpha\{112\}$ silicide plane. In case of $\beta\{100\}\|Si\{100\}$ habit plane, the alignment $[010]_\beta$ along $[001]_{Si}$ results in the NCS density of 0.281, whereas alignment $[010]_\beta$ along $[011]_{Si}$ direction demonstrates a complex NCS map with very low NCS density equal to 0.037. The $\beta\{100\}\|\alpha\{001\}$ ORs has lower values of the NSC density, 0.044 and 0.079 for $[010]_\beta\|[001]_{Si}$ and $[010]_\beta\|[011]_{Si}$, respectively. From this simple consideration of the NCS map, one can conclude that the $\beta\{110\}\|\alpha\{112\}$ habit planes and $\beta\{101\}\|\alpha\{112\}$ ones along with $\beta\{100\}[010]\|Si\{100\}[110]$ OR are more favourable for epitaxy, where a maximum of the NCS density appears for the latter OR.

Moreover, a condition of the parallelism of the best matching pairs of planes $\beta(422)$ and $\alpha(012)$ (Table 1) should be taking into account as well. In such way, the

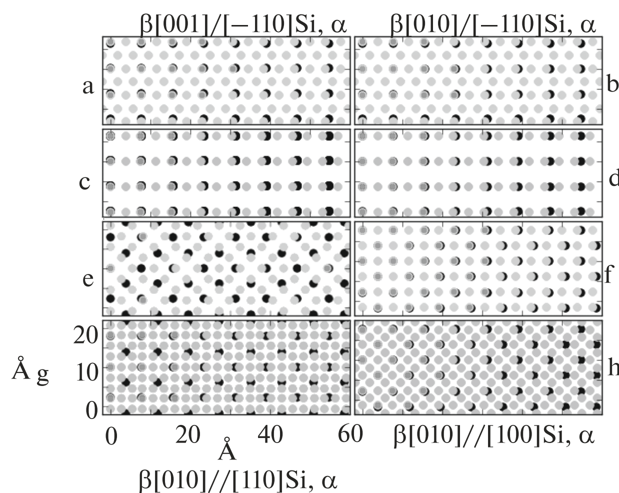

Fig. 1. Near coincidence site map for conventional ORs between β-$FeSi_2$ and Si or α-$FeSi_2$. Fig1 (a) corresponds to $\beta\{110\}\|Si\{111\}$ habit plane, (b) $\beta\{101\}\|Si\{111\}$, (c) $\beta\{110\}\|\alpha\{112\}$, (d) $\beta\{101\}//\alpha\{112\}$, (e) $\beta\{100\}[010]\|Si\{001\}[100]$, (f) $\beta\{100\}[010]\|Si\{100\}[110]$, (g) $\beta\{100\}[010]//\alpha\{001\}[100]$, (h) $\beta\{100\}[010]//\alpha\{001\}[110]$. Black solid circles depict atoms in β-$FeSi_2$ silicide plane; yellow ones are atoms in silicon planes, cyan ones correspond to α-$FeSi_2$ and solid red circles portray near coincidence sites with the criterion of 10.8% of the silicon lattice parameter in RT.

only β-$FeSi_2$//α-$FeSi_2$ OR containing $\beta(422)$ and $\alpha(012)$ planes met at the interface with $\beta[040]$ parallel to $\alpha[110]$, among ORs already regarded, is $\beta\{100\}[010]//\alpha\{001\}[110]$. In turn at $\beta\{110\}\|\alpha\{112\}$ and $\beta\{101\}\|\alpha\{112\}$ alignment the planes $\beta(422)$ and $\alpha(012)$ do not contain high-density atomic rows parallel to each other. Figure 2 (right panel) illustrates the location of these planes at the schematic illustration of a layer stack with the OR denoted. For the $\beta\{100\}\|\alpha\{001\}$ OR, the misfits between $\beta[010]$ and $\alpha\langle 220\rangle$, $\beta[001]$ and $\alpha\langle 220\rangle$, $\beta[011]$ and $\alpha\langle 400\rangle$ are 2.83, 3.01 and 2.92%, respectively. In case of the $\beta\{101\}\|\alpha\{112\}$ OR (Fig. 3b), the highly packed atomic rows at the interface are $\beta[001]$ and $\alpha\langle 220\rangle$. The misfit is 3.014%, whereas angle between $\beta\langle 111\rangle$ and $\alpha\langle 021\rangle$ belonging to $\beta(422)$ and $\alpha(012)$ planes, respectively, equals to 1.111° which does not result to the good epitaxy conditions prescribed by the edge-to-edge or plane-to-plane matching model. Thus, the $\beta\{100\}[010]//\alpha\{001\}[110]$ OR requires more detailed consideration of the NCS maps.

From Fig. 2 one can see that β-$FeSi_2$ cell has three non-equivalently packed {100} planes, where the $\beta(200)$, $\beta(400)$ planes are packed with only Fe atoms and $\beta(2.7\ 0\ 0)$ with silicon ones. While in Figures 1e–1h the β//Si and $\beta//\alpha$ NCS maps for the $\beta(400)$ plane are represented, Fig. 3 represents the NCS maps for the $\beta(200)$ plane (left column) and the $\beta(2.7\ 0\ 0)$ plane (right column). Thus, the superimposition of $\beta(200)$ plane with the Si(001) one gives us the NCS density of

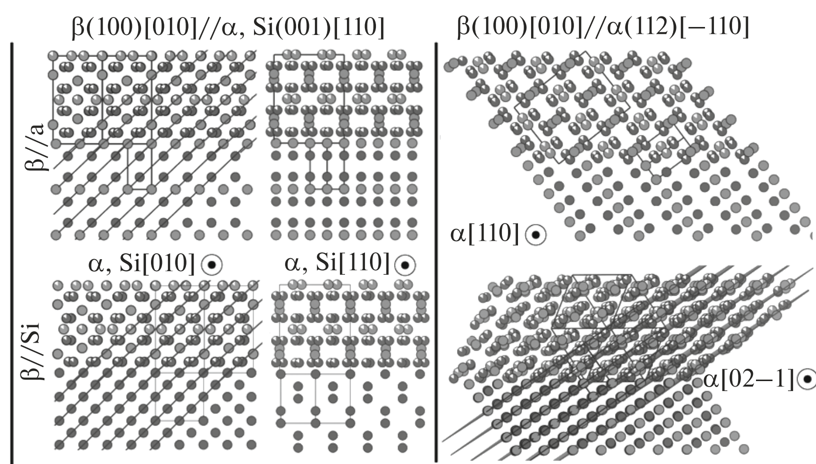

Fig. 2. Schematic illustration of epitaxial alignment β{100}[010]//Si{001}[110] (left panel, upper scheme), β{100}[010]//α{001}[110] (left column, lower scheme), β(101)[010]//α(112)[−110] (right panel).

0.289. In case of the β(200) and α(001) plane the NCS density is 0.124, whereas this value for β(2.7 0 0)‖Si(001) is 0.225 and the β(2.7 0 0)‖α(001) habit planes result in 0.318, i.e. the highest NCS density value among the considered β‖Si and β‖α habit planes. Thus, we suppose that the β(2.7 0 0)‖α(001) habit plane can be considered as the best matching and can be corresponded to the lowest interfacial energy or minimum elastic energy according to the principles of geometric models applied here. Comparison of larger area NCS maps (200 × 200 Å) for three non-equivalent β{100} planes superimposed with Si(001) and α(001) planes is given in supplementary material (Fig. S1).

However, the interatomic spacing misfit of close-packed atomic rows in the β(2.7 0 0)[010]‖α{001}[110] OR considered above is not the least among observed and equal to 2.89% (Table 1). The least interatomic

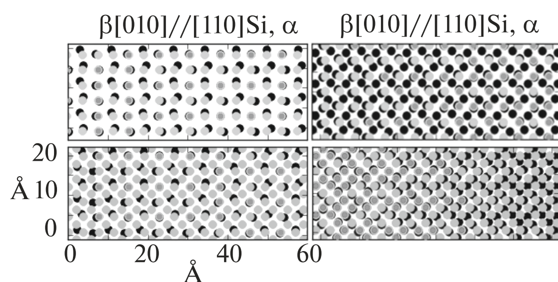

Fig. 3. Comparison of near coincidence site maps for β(2 0 0)[010]‖Si{001}[110] and β(2 0 0)[010]‖α{001}[110] habit planes (left panel). Right panel contains NCS maps for β(2.7 0 0)[010]‖Si{001}[110] and β(2.7 0 0)[010]‖α{001}[110]. Black solid circles depict atoms in β-$FeSi_2$ silicide plane; yellow ones are atoms in silicon planes, cyan ones correspond to α-$FeSi_2$ and solid red circles portray near coincidence sites with the criterion of 10.8% of the silicon lattice parameter in RT.

spacing misfit observed for α-, β-$FeSi_2$ phases corresponds to the β[−120]//α [4−42] directions belonging to β(422)//α(012) planes and has a value of 0.87%. Thus, additional consideration of possible interfaces where β(422)[−120]//α(012) [4−42] OR would play a key role seems to be reasonable.

Calculation of NCS density profiles at rotation around α [4−42] or β[−120] directions for β(422)[−120]//α(012) [4−42] OR (Fig. 4a) gives reason to believe that habit planes observed at θ = 0° and 33.8° could be considered as a basis for the axiotaxial alignment [59]. The θ is the deviation angle from an initial plane. In case of the growth of β-$FeSi_2$ on α-$FeSi_2$ phase, a high value of NCS density is observed at these angles. Since a high value of the NCS density could be caused by a few atoms in planes taken into account, the calculation was conducted under four criteria. First and second ones are thicknesses of the layer, inside of which the NCS are searched (0.2 and 1 Å), and the third and fourth are a consideration concerning the layer atom quantity of which phase, α- or β-$FeSi_2$, the NCS density is calculated. Thus, the calculation within 0.2 Å thickness layer gives rise to the NCS density of about 0.6° and 0.4° at angle 33.8°, and 0.3° at 0° for β-, and α-$FeSi_2$ phases respectively. Other angles, where high NCS density values are observed, demonstrate diminishing of NCS density value when the calculation at 1 Å thickness layer is applied (Fig. 4a). However, NCS densities at 0° and 33.8° angles remain the highest over the whole range.

The NCS map corresponded to β(4 2 7.0216) [−120]‖α(−1.23 0.923 4.305) [4−42] (θ = 33.8°) OR with identical OR with α-$FeSi_2$ demonstrates higher NCS density than equivalent β‖Si habit plane (Fig. 4b). (Fig. 4b, where the habit plane corresponded to the case when θ = 33.8°, as a comparison NCS map for the equivalent habit plane of β-$FeSi_2$ and

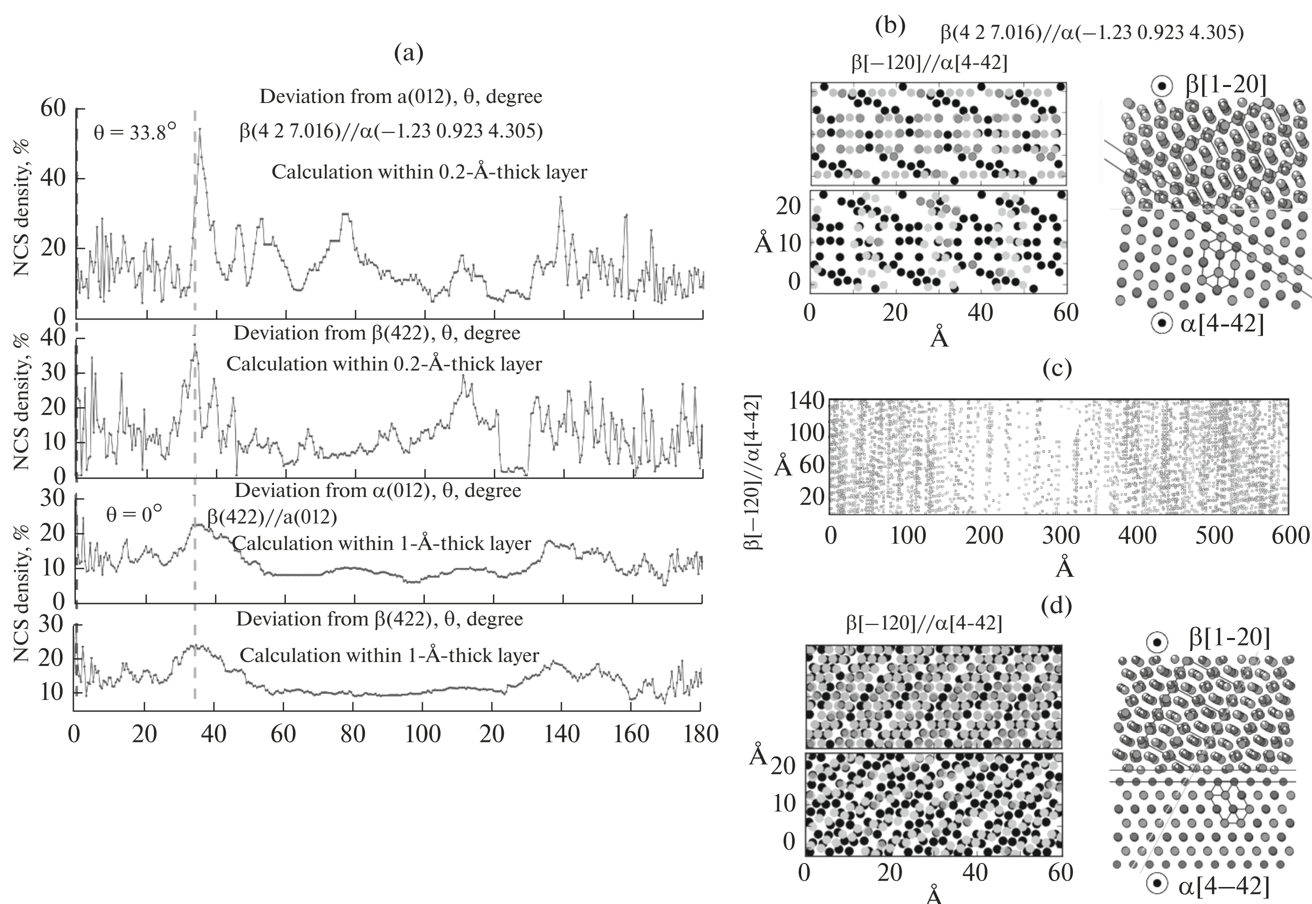

Fig. 4. (a) NCS density profiles at rotation around α [4–42] or β[-120] directions for β(422)[–120]//α(012) [4–42] $d_{\text{test layer}}$ = 0.2 and 1 Å, (b) NCS map and schematic illustration of axiotaxial alignment in β(422)[–120]//α(012) [4–42] system with β(4 2 7.0216)‖α(–1.23 0.923 4.305) habit plane corresponded to the case when θ = 33.8°, as a comparison NCS map for the equivalent habit plane of β-$FeSi_2$ and silicon is given, (c) Large scale NCS map for β(4 2 7.0216)[–120]‖α(–1.23 0.923 4.305) [4–42] habit plane calculated for two 0.2 Å thickness layers situated in 2 Å from each other. Blue and red circles depict near coincidence sites in these layers. (d) NCS map and schematic illustration of axiotaxial alignment in β(422)[–120]//α(012) [4–42] system with β(422)‖α(012) habit plane corresponded to the case when θ = 0°, as a comparison NCS map for the equivalent habit plane of β-$FeSi_2$ and silicon is given. Black solid circles depict atoms in β-$FeSi_2$ silicide plane; yellow ones are atoms in silicon planes, cyan ones correspond to α-$FeSi_2$ and solid red circles portray NCS with the criterion of 10.8% of the silicon lattice parameter in RT.

silicon is given). One can assume that a heterosystem having the β(4 2 7.0216) [–120] ‖α(–1.23 0.923 4.305) [4–42] habit plane (θ = 33.8°) could tend to form stepped interface. The NCS maps for the given β(4 2 7.0216)‖α(–1.23 0.923 4.305) OR calculated in interval layer of 2 Å (Fig. 4c, the habit plane calculated for two 0.2 Å thickness layers situated in 2 Å from each other) shows that NCS density can be increased about two times due to the formation of the stepped interface. In turn, the β(4 2 2)[–120]‖α(012) [4–42] (θ = 0°) habit plane demonstrates a dense NCS zone spread along β[–120] direction (Fig. 4d, the habit plane corresponded to the case when θ = 0°, as a comparison NCS map for the equivalent habit plane of β-$FeSi_2$ and silicon is given). Large-scale NCS maps for both OR considered (Figs. S2a, S2b) show that such NCS zone spread over 150 Å. Thus, one can expect a formation of prolonged β-$FeSi_2$ nanoislands with a high aspect ratio on the α-$FeSi_2$ surface mentioned above.

Above we have considered the habit planes where the planes with smallest interplanar β(4 2 2)//α(012) and interatomic β[–120]‖α [4–42] distance were parallel to each other. According to the edge-to-edge model, the planes with the closest interplanar distance can be not parallel to each other and merely bring atoms in close-packed atomic rows to meet at the interface. Results obtained show that the application of the unfixed condition for the aligning planes does not result to a remarkable increase in NCS density in comparison with plane-to-plane model and remains in 0.3–0.4 range (Figs. S2c, S2d).

2.3. On the Issue of Targeted α-,γ- or s-$FeSi_2$ Phase Growth on the Silicon Surface

As a result of consideration of NCS density for different habit planes in β-$FeSi_2$//α-, γ-, *s*-$FeSi_2$ heterosystems we suppose that β-$FeSi_2$//α-$FeSi_2$ pair has more advantages for the formation of less strained

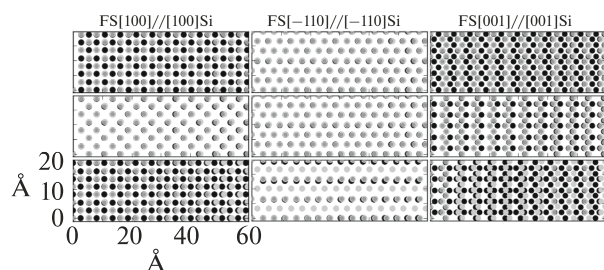

Fig. 5. Near coincidence site map for low-index habit planes between Si and s-$FeSi_2$ (upper row), Si and γ-$FeSi_2$ (middle row), Si and α-$FeSi_2$ (lower row). First column correspond to Si{001}//FS{001} habit plane, second one—Si{111}//FS{111}, in case α-$FeSi_2$—Si{111}//α{112}, third one—Si{110}//FS{110}. Black solid circles depict atoms in silicide plane; yellow ones are atoms in silicon planes and solid red circles depict near coincidence sites with the criterion of 10.8% of the silicon lattice parameter in RT.

β-$FeSi_2$ phase nanocrystals. Thus, the synthesis process should contain two main stages; one is the preparation of α-$FeSi_2$ seeds with an atomically flat α(001) surface adjacent to vacuum, which can be considered to be easier to form in comparison to other α-$FeSi_2$ planes with high NCS density described in 2.1. The second is the preparation of the β-$FeSi_2$ phase on the α-$FeSi_2$ seed surface. However, taking into account smaller interplanar and interatomic misfit value of γ-, and *s*-$FeSi_2$/Si heterosystems (Table 1) it is more favourable for s-, or γ-$FeSi_2$ phases to grow on the silicon surface. The NCS maps for α-, γ-, and *s*-$FeSi_2$ interfaces with silicon (Fig. 5) also indicate advantages of the γ-, and *s*-$FeSi_2$ formation on the low Miller index (001), (111), (110) silicon surfaces. Thus, superimposition of α{112}, α{110} planes with Si{111}, Si{110} surfaces, respectively, yields to both γ-, and *s*-$FeSi_2$ phases, where the NCS density for them reaches the value of 1 for 20 × 60 Å area. In turn, the NCS densities for α{112}//Si{111} and α{110}//Si{110} are 0.57 and 0.26, respectively. Whereas, in case of the Si{001}//α{001} habit plane, α-$FeSi_2$ demonstrates an increase of NCS density up to 0.82 comparable to 1 corresponded to γ, and *s*-$FeSi_2$ case. It should be noted that *s*-$FeSi_2$ compound with CsCl structure is shown without atom vacancies, which should result in $FeSi_2$ stoichiometry. Thus, one should bear in mind that some black circles should be missing in the pictures for *s*-$FeSi_2$.

It is seen that γ-$FeSi_2$ compound is at an advantage due to its *Fm*3*m* space group in front of both α-, and *s*-$FeSi_2$. No atoms from γ-silicide have missing atoms in silicon plane as it happens for the Si{001}//α,s{001} habit planes. Thus, from the geometrical model applied here one should consider γ-$FeSi_2$ as a more favourable for growth on Si(001) surface. Experimental consideration of the $FeSi_2$ silicide formation on silicon substrate shows contradictory results as we have already noticed in the introduction. In the temperature range of 600–750°C the formation of all three phases were reported [22, 28, 30, 31, 40]. This indicates competitiveness of their formation, where particular conditions of the synthesis (growth technique,

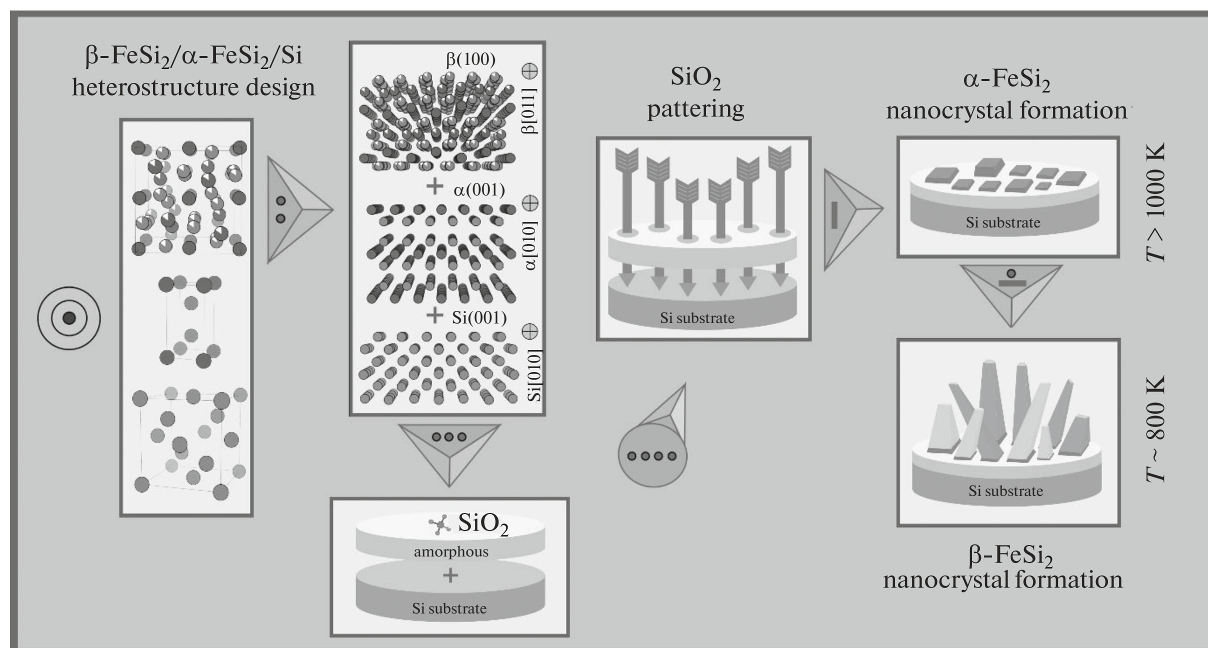

Fig. 6. Schematic drawing illustrating the design and technological procedure for β-$FeSi_2$/α-$FeSi_2$/Si heterostructure.

deposition rates, silicon surface thermal history, slight changes in the temperature), determine whether one or another phase tends to be grown. One way to control phase formation is the temperature. It is known that the $\alpha(110)//Si(022)$ misfit value can approach 0% around 1000–1100 K according to the works [32, 56, 59]. Thus, the temperature should drastically affect the preferable formation of α-$FeSi_2$ or γ-$FeSi_2$ phases on the silicon surface. It is more probable to observe γ-$FeSi_2$ (or *s*-$FeSi_2$) growth under the low temperature [22, 27–31] and growth α-$FeSi_2$ at temperatures above 1000 K [32, 56, 59].

CONCLUSIONS

Semiconducting iron disilicide phase β-$FeSi_2$ as acting material in optoelectronic devices, in particular, the light-emitting diodes working at the optical communication wavelength of 1.5 μm, is coveted by many researchers. However, it lacks such flexibility and versatility as the conventionally used InGaAs semiconductors. Hence, it appears to be important to find new approaches for engineering crystal and band structure of β-$FeSi_2$, e.g. via nanopatterning or lattice strain. Here, we have discussed possibilities of growing β-$FeSi_2$ phase on α-$FeSi_2$ from the point of view of the crystallogeometrical approaches. Based on analysis of interplanar and interatomic misfit of different silicide/silicon and silicide/silicide (α-, β, γ-, *s*-$FeSi_2$) pair, the α-$FeSi_2$ phase appeared to be the most suitable as a buffer layer between the Si and β-$FeSi_2$ phases. Through the consideration of the near coincidence site density of the possible conventional and predicted β-$FeSi_2$/α-$FeSi_2$ interfaces in comparison with the β-$FeSi_2$/Si ones we established the $\alpha(001)$ surface as one of the suitable surfaces for further growth of β-$FeSi_2$ phase. It shows the higher NCS density and might facilitate the growth β-$FeSi_2$ phase on silicon. Being metastable α-$FeSi_2$ phase competes with others, such as γ-$FeSi_2$ and *s*-$FeSi_2$, during the growth on a silicon substrate. Thus, the temperature may be utilised for the alternation of the phase formation sequence during the technological procedures. Thus, a possible heterostructure design consisting of only silicon and iron silicide intended to customise the β-$FeSi_2$ band structure characteristics has been proposed (Fig. 6).

FUNDING

The work was supported by Russian Foundation for Basic Research, Government of Krasnoyarsk Territory, Krasnoyarsk Regional Fund of Science to the research project no. 18-42-243013. The work was partially supported by the Ministry of Education and Science of the Russian Federation and by Siberian Branch of the Russian Academy of Sciences (Project II.8.70).

REFERENCES

1. I. A. Tarasov, Z. I. Popov, S. N. Varnakov, M. S. Molokeev, A. S. Fedorov, I. A. Yakovlev, et al., JETP Lett. **99,** 565 (2014). https://doi.org/10.1134/S0021364014100105
2. S. G. Ovchinnikov, S. N. Varnakov, S. A. Lyashchenko, I. A. Tarasov, I. A. Yakovlev, E. A. Popov, et al., Phys. Solid State **58,** 2277 (2016). https://doi.org/10.1134/S1063783416110299
3. I. A. Yakovlev, I. A. Tarasov, and S. A. Lyashchenko, J. Magn. Magn. Mater. **440,** 161 (2016). https://doi.org/10.1016/j.jmmm.2016.12.051
4. H. Tokushige, T. Endo, K. Hiidome, K. Saiki, S. Kitamura, T. Katsuyama, et al., Jpn. J. Appl. Phys. **54,** 07JB03 (2015). https://doi.org/10.7567/JJAP.54.07JB03
5. Z. Liu, S. Wang, N. Otogawa, Y. Suzuki, M. Osamura, Y. Fukuzawa, et al., Sol. Energy Mater. Sol. Cells. **90,** 276 (2006). https://doi.org/10.1016/j.solmat.2005.03.014
6. Y. Gao, H. W. Liu, Y. Lin, and G. Shao, Thin Solid Films **519,** 8490 (2011). https://doi.org/10.1016/j.tsf.2011.05.030
7. M. Mohebali, Y. Liu, L. Tayebi, J. S. Krasinski, and D. Vashaee, Renewable Energy **74,** 940 (2015). https://doi.org/10.1016/j.renene.2014.08.059
8. W. Li, C. Wen, M. Yamashita, T. Nonomura, Y. Hayakawa, and H. Tatsuoka, J. Cryst. Growth **340,** 51 (2012). https://doi.org/10.1016/j.jcrysgro.2011.11.059
9. J. Theis, R. Bywalez, S. Küpper, A. Lorke, and H. Wiggers, J. Appl. Phys. **117,** 054303 (2015). https://doi.org/10.1063/1.4906500
10. D. Leong, M. Harry, K. J. Reeson, and K. P. Homewood, Nature **387,** 686 (1997). https://doi.org/10.1038/42667
11. Y. Maeda, Appl. Surf. Sci. **254,** 6242 (2008). https://doi.org/10.1016/j.apsusc.2008.02.127
12. D. Z. Chi, Thin Solid Films **537,** 1 (2013). https://doi.org/10.1016/j.tsf.2013.04.020
13. N. G. Galkin, E. A. Chusovitin, D. L. Goroshko, A. V. Shevlyagin, A. A. Saranin, T. S. Shamirzaev, et al., Appl. Phys. Lett. **101,** 163501 (2012). https://doi.org/10.1063/1.4758485
14. Y. Ando, A. Imai, K. Akiyama, Y. Terai, and Y. Maeda, Thin Solid Films **515,** 8133 (2007). https://doi.org/10.1016/j.tsf.2007.02.024
15. Y. Maeda, T. Tatsumi, Y. Kawakubo, Y. Noguchi, H. Kobayashi, K. Narumi, et al., Phys. Status Solidi C **11,** 1626 (2014). https://doi.org/10.1002/pssc.201400039
16. A. V. Shevlyagin, D. L. Goroshko, E. A. Chusovitin, S. A. Balagan, S. A. Dotcenko, K. N. Galkin, et al., J. Appl. Phys. **121,** 113101 (2017). https://doi.org/10.1063/1.4978372

17. M. Suzuno, T. Koizumi, and T. Suemasu, Appl. Phys. Lett. **94,** 213509 (2009). . https://doi.org/10.1063/1.3147168
18. Roithner LaserTechnik GmbH, Price list 03/2017. http://www.roithner-laser.com/pricelist.pdf
19. J. W. Hwang, B. K. Kim, S. J. Lee, M. H. Bae, and J. C. Shin, Curr. Appl. Phys. **15,** S35 (2015). https://doi.org/10.1016/j.cap.2015.04.014
20. D. Van Dam, D. R. Abujetas, R. Paniagua-Domínguez, J. A. Sánchez-Gil, E. P. A. M. Bakkers, J. E. M. Haverkort, et al., Nano Lett. **15,** 4557 (2015). https://doi.org/10.1021/acs.nanolett.5b01135
21. S.-W. Hung, P. -H. Yeh, L. -W. Chu, C.-D. Chen, L.-J. Chou, Y. -J. Wu, et al., J. Mater. Chem. **21,** 5704 (2011). . https://doi.org/10.1039/c1jm10232j
22. S. Liang, R. Islam, D. J. Smith, and P. A. Bennett, J. Cryst. Growth **295,** 166 (2006). https://doi.org/10.1016/j.jcrysgro.2006.05.076
23. K. Yamamoto, H. Kohno, S. Takeda, and S. Ichikawa, Appl. Phys. Lett. **89,** 83107 (2006). https://doi.org/10.1063/1.2338018
24. L. Chen and W. Wu, Jpn. J. Appl. Phys. **54,** 07JA04 (2015). https://doi.org/10.7567/JJAP.54.07JA04
25. G. Shao, Y. Gao, X. H. Xia, and M. Milosavljević, Thin Solid Films **519,** 8446 (2011). https://doi.org/10.1016/j.tsf.2011.05.036
26. Y. Gao, G. Shao, R. S. Chen, Y. T. Chong, and Q. Li, Solid State Commun. **149,** 97 (2009). https://doi.org/10.1016/j.ssc.2008.11.002
27. H. von Känel, K. A. Mäder, E. Müller, N. Onda, and H. Sirringhaus, Phys. Rev. B: Condens. Matter **45,** 13807 (1992). https://doi.org/10.1103/PhysRevB.45.13807
28. I. Goldfarb, Y. Camus, M. Dascalu, F. Cesura, R. Chalasani, and A. Kohn, Phys. Rev. B **96,** 45415 (2017). https://doi.org/10.1103/PhysRevB.96.045415
29. H. von Känel, N. Onda, H. Sirringhaus, E. Müller-Gubler, S. Goncalves-Conto, and C. Schwarz, Appl. Surf. Sci. **70–71,** 559 (1993). https://doi.org/10.1016/0169-4332(93)90579-Z
30. A. L. V. de Parga, J. de la Figuera, C. Ocal, and R. Miranda, Ultramicroscopy **42–44,** 845 (1992). https://doi.org/10.1016/0304-3991(92)90367-S
31. D. Das, J. C. Mahato, B. Bisi, B. Satpati, and B. N. Dev, Appl. Phys. Lett. **105,** 191606 (2014). https://doi.org/10.1063/1.4901815
32. G. Cao, D. J. Singh, X. -G. Zhang, G. Samolyuk, L. Qiao, C. Parish, et al., Phys. Rev. Lett. **114,** 147202 (2015). https://doi.org/10.1103/PhysRevLett.114.147202
33. N. Jedrecy, A. Waldhauer, M. Sauvage-Simkin, R. Pinchaux, and Y. Zheng, Phys. Rev. B **49,** 4725 (1994). https://doi.org/10.1103/PhysRevB.49.4725
34. J. Chevrier, P. Stocker, L. T. Vinh, J. M. Gay, and J. Derrien, Europhys. Lett. **22,** 449 (1993). . https://doi.org/10.1209/0295-5075/22/6/009
35. X. W. Lin, M. Behar, J. Desimoni, H. Bernas, J. Washburn, and Z. Liliental-Weber, Appl. Phys. Lett. **63,** 105 (1993). https://doi.org/10.1063/1.109727
36. S. S. Pan, C. Ye, X. M. Teng, H. T. Fan, and G. H. Li, Phys. Status Solidi A **204,** 3316 (2007). https://doi.org/10.1002/pssa.200622438
37. C. Detavernier, C. Lavoie, J. Jordan-Sweet, and A. S. Özcan, Phys. Rev. B **69,** 174106 (2004). https://doi.org/10.1103/PhysRevB.69.174106
38. J. K. Tripathi, G. Markovich, and I. Goldfarb, Appl. Phys. Lett. **102,** 251604 (2013). https://doi.org/10.1063/1.4812239
39. B.-X. Xu, Y. Zhang, H. -S. Zhu, D.-Z. Shen, and J.-L. Wu, Mater. Lett. **59,** 833 (2005). https://doi.org/10.1016/j.matlet.2004.10.060
40. Z.-Q. Zou, X. Li, X.-Y. Liu, K.-J. Shi, and X.-Q. Guo, Appl. Surf. Sci. **399,** 200 (2017). https://doi.org/10.1016/j.apsusc.2016.12.056
41. V. E. Borisenko, *Semiconducting Silicides* (Springer, Berlin, 2000). https://doi.org/10.1007/978-3-642-59649-0
42. J. H. Van Der Merwe, G. J. Shiflet, and P. M. Stoop, Metall. Trans. A **22,** 1165 (1991). https://doi.org/10.1007/BF02660648
43. S. Shao, J. Wang, and A. Misra, J. Appl. Phys. **116,** 023508 (2014). https://doi.org/10.1063/1.4889927
44. P. M. Kelly and M. X. Zhang, Metall. Mater. Trans. A **37,** 833 (2006). https://doi.org/10.1007/s11661-006-0056-4
45. M. X. Zhang and P. M. Kelly, Acta Mater. **53,** 1073 (2005). https://doi.org/10.1016/j.actamat.2004.11.007
46. Q. Liang and W. T. Reynolds, Metall. Mater. Trans. A **29,** 2059 (1998). https://doi.org/10.1007/s11661-998-0032-2
47. B. Aronsson, D. H. Templeton, S. Rundqvist, E. Varde, and G. Westin, Acta Chem. Scand. **14,** 1414 (1960). https://doi.org/10.3891/acta.chem.scand.14-1414
48. H. Yamane and T. Yamada, J. Alloys Compd. **476,** 282 (2009). https://doi.org/10.1016/j.jallcom.2008.08.078
49. X. F. Gu, T. Furuhara, and W. Z. Zhang, J. Appl. Crystallogr. **49,** 1099 (2016). https://doi.org/10.1107/S1600576716006075
50. N. Miyano, K. Ameyama, and G. C. Weatherly, ISIJ Int. **40,** S199 (2000).
51. T. Furuhara, T. Maki, and K. Oishi, Metall. Mater. Trans. A **33,** 2327 (2002). https://doi.org/10.1007/s11661-002-0356-2
52. F. Ye, W. Z. Zhang, and D. Qiu, Acta Mater. **54,** 5377 (2006). https://doi.org/10.1016/j.actamat.2006.07.006
53. A. R. S. Gautam and J. M. Howe, Philos. Mag. **91,** 3203 (2011). https://doi.org/10.1080/14786435.2011.573817
54. X. Wang, H. Huang, X. Gu, Y. Li, Z. Jia, and Q. Liu, J. Appl. Crystallogr. **49,** 1223 (2016). https://doi.org/10.1107/S160057671600933X
55. I. A. Yakovlev, I. A. Tarasov, M. V. Rautskii, and M. N. Volochaev, Semiconductors **52,** 654 (2018). https://doi.org/10.1134/S1063782618050330

56. I. A. Tarasov, I. A. Yakovlev, M. S. Molokeev, M. Rautskii, I. V. Nemtsev, S. N. Varnakov, and S. G. Ovchinnikov, Mater. Lett. **168,** 90 (2016). https://doi.org/10.1016/j.matlet.2016.01.033

57. I. A. Tarasov, N. N. Kosyrev, S. N. Varnakov, S. G. Ovchinnikov, S. M. Zharkov, V. A. Shvets, et al., Tech. Phys. **57,** 1225 (2012). . https://doi.org/10.1134/S1063784212090241

58. I. A. Tarasov, M. A. Visotin, A. S. Aleksandrovsky, N. N. Kosyrev, I. A. Yakovlev, M. S. Molokeev, A. V. Lukyanenko, A. S. Krylov, A. S. Fedorov, S. N. Varnakov, and S. G. Ovchinnikov, J. Magn. Magn. Mater. **440,** 144 (2017). https://doi.org/10.1016/j.jmmm.2016.12.084

59. C. Detavernier, C. Lavoie, J. Jordan-Sweet, and A. S. Özcan, Phys. Rev. B. **69,** 174106 (2004). https://doi.org/10.1103/PhysRevB.69.174106

60. M. Imai, Y. Isoda, and H. Udono, Intermetallics **67,** 75 (2015). https://doi.org/10.1016/j.intermet.2015.07.015

61. F. Zhang and S. Saxena, Scr. Mater. **54,** 1375 (2006). https://doi.org/10.1016/j.scriptamat.2005.11.076

62. G. Kresse and J. Furthmüller, Phys. Rev. B **54,** 11169 (1996). https://doi.org/10.1103/PhysRevB.54.11169

63. G. Kresse and J. Hafner, Phys. Rev. B **47,** 558 (1993). https://doi.org/10.1103/PhysRevB.47.558

64. P. E. Blöchl, Phys. Rev. B **50,** 17953 (1994). https://doi.org/10.1103/PhysRevB.50.17953

65. J. D. Pack and H. J. Monkhorst, Phys. Rev. B **16,** 1748 (1977). https://doi.org/10.1103/PhysRevB.16.1748

66. L. L. Boyer, Phys. Rev. Lett. **42,** 584 (1979). https://doi.org/10.1103/PhysRevLett.42.584

67. R. E. Allen, F. W. De Wette, and A. Rahman, Phys. Rev. **179,** 887 (1969). https://doi.org/10.1103/PhysRev.179.887

68. A. Togo and I. Tanaka, Scr. Mater. **108,** 1 (2015). https://doi.org/10.1016/j.scriptamat.2015.07.021

69. A. Togo, L. Chaput, I. Tanaka, and G. Hug, Phys. Rev. B: Condens. Matter Mater. Phys. **81,** 1 (2010). . https://doi.org/10.1103/PhysRevB.81.174301

70. A. Jain and A. J. H. McGaughey, Comput. Mater. Sci. **110,** 115 (2015). https://doi.org/10.1016/j.commatsci.2015.08.014

71. J. P. Perdew, A. Ruzsinszky, G. I. Csonka, O. A. Vydrov, G. E. Scuseria, L. A. Constantin, et al., Phys. Rev. Lett. **100,** 136406 (2008). . https://doi.org/10.1103/PhysRevLett.100.136406

72. J. P. Perdew, K. Burke, and M. Ernzerhof, Phys. Rev. Lett. **77,** 3865 (1996). https://doi.org/10.1103/PhysRevLett.77.3865

73. H. Ibach, Phys. Status Solidi B **31,** 625 (1969). https://doi.org/10.1002/pssb.19690310224

74. Y. Okada and Y. Tokumaru, J. Appl. Phys. **56,** 314 (1984). https://doi.org/10.1063/1.333965

75. U. Starke, W. Weiss, M. Kutschera, R. Bandorf, and K. Heinz, J. Appl. Phys. **91,** 6154 (2002). https://doi.org/10.1063/1.1467397